First principles calculations of X-ray absorption in an ultrasoft pseudopotentials scheme: from α-quartz to high-T_c compounds.

Christos Gougoussis, Matteo Calandra, Ari P. Seitsonen, and Francesco Mauri
CNRS and Institut de Minéralogie et de Physique des Milieux condensés, case 115, 4 place Jussieu, 75252, Paris cedex 05, France

(Dated: June 29, 2009)

We develop a first-principles scheme based on the continued fraction approach and ultrasoft pseudopotentials to calculate K-edge X-ray absorption spectra in solids. The method allows for calculations of K-edge X-ray absorption spectra in transition metal and rare-earths compounds with substantially reduced cutoffs respect to the norm-conserving case. We validate the method by calculating Si and O K-edges in α quartz, Cu K-edge in Copper and in La_2CuO_4. For the case of Si and O edges in α quartz and in Copper we obtain a good agreement with experimental data. In the Cu K-edge spectra of La_2CuO_4, a material considered a real challenge for density functional theory we attribute all the near-edge and far-edge peaks to single particle excitations.

PACS numbers: 74.70.Ad, 74.25.Kc, 74.25.Jb, 71.15.Mb

I. INTRODUCTION

With the development of synchrotron radiation sources, X-ray absorption spectroscopy (XAS) has become a very powerful and a widely used technique to investigate structural properties and electronic structures in condensed matter physics. Since the absorption of X-rays at well-suited energies is chemical and orbital selective, it is possible to probe electronic excitations and explore the local environment around the absorbing atom. The use of polarized X-rays allows to separate the contributions of different atomic orbitals through the study of angular dependence of the spectra.[1]

K-edge XAS has been used to study the electronic structure of correlated transition metal compounds,[2,3,4], to probe the local environment around impurities in crystals[5] and in disordered matter like glass or liquids. For instance, XAS plays a crucial role for the understanding of the microscopic structure of water[6,7,8,9,10,11]. The widespread use of XAS as a structural utility and as a probe of the electronic structure requires reliable theoretical approaches to interpret the measured spectra.

Different theoretical methods are available to calculate XAS. The multiplet approach[12], used to calculate pre-edge features for systems with localized final states, relies on the solution of a few-sites manybody hamiltonian including several parameters that are suitably chosen to fit the experimental data. This approach, although providing a full manybody solution to the problem, has three main shortcomings; (i) it is limited to pre-edge structures and (ii) non-local excitations are hardly taken into account due to the short-range nature of the considered clusters, (iii) in some cases a small variation of the hamiltonian parameters leads to substantially different spectra. The multiple scattering approach[13,14,15] and its extension to non muffin-tin potentials have been widely used with success, but these methods are not based on first principles and require adjustable parameters to interpret the experimental data. The solution of the Bethe Salpeter equation is the first principle method having the most satisfactory treatment of many-body effects[16]. However being this method extremely time consuming it only allows for a description of the pre-edge region of the XAS spectra: the near-edge and far-edge regions cannot be easily computed.

Density functional theory (DFT) approaches[17,18,19,20,21,22], have been successfully applied to K-edges of weakly correlated materials. In a pseudopotential framework, the use of the PAW[18] method allows to reconstruct the all electron wavefunction and consequently to obtain XAS intensities unaffected by the presence of a pseudopotential. Furthermore the development of a DFT method[17] using norm-conserving pseudopotentials and based on the continued fraction approach permits to obtain XAS spectra up to the far edge region. Another advantage of DFT approaches is that they allow for structural optimization of the local environment around the absorbing atom, a key issue in the case of impurities or defects.

In time-independent DFT methods, core-hole effects are included in a supercell approach by generating a pseudopotential with a core-hole in the desired atomic core level. While this method works very well for weakly correlated system, in the presence of moderate or strong correlation it has two main shortcomings. The first is the unsatisfactory treatment of electron-electron interaction in the DFT functional. The second is the large increase in computational time when dealing with transition metals and rare-earths mainly related to the huge kinetic energy cutoffs involved and the need to simulate large supercells with reduced symmetry .[50] A partial remedy for the lack of correlation effects is the use of the DFT+U approximation[23]. Recently the method of ref.[17] was generalized to the DFT+U approximation[4]. It was shown the DFT+U dramatically improves the agreement with experimental data in the pre-edge region of correlated 3d transition metal compounds[4]. Still the second problem holds, namely the huge cutoffs needed to simulate transition metal and rare-earth compounds require a substantial computational time.

In this work we solve this problem developing a method to calculate XAS in an Ultrasoft pseudopotential[24] scheme and relying on the continued fraction approach. US pseudopotentials allow for small cutoffs (20-40 Ry) even for transition-metals and rare earth systems, contrary to norm-conserving ones. Thus the use of these pseudopotentials reduces the computational cost of the supercell calculation by an order of magnitude. The drawback is that the continued fraction scheme developed in ref.[17] does not apply if at least one ultrasoft pseudopotential (not necessary the absorbing atom) is present in the calculation. For this reason we reformulate completely the continued fraction and the corresponding lanczos approach in a way that is suitable for Ultrasoft pseudopotentials. We then apply the method to Si and O K-edge in $\alpha-$quartz, to Cu K-edge in copper and in La_2CuO_4 and compare the results with available experimental data.

The structure of the paper is the following. In secs. II and III we remind the general expression of the XAS cross section within the projector augmented wave formalism. In sec. IV and V we develop the continued fraction approach in the case of ultrasoft pseudopotentials, and finally in sec. VI we apply the method to the aforementioned systems.

II. X-RAY ABSORPTION CROSS-SECTION

The XAS cross section is[1] :

$$\sigma(\omega) = 4\pi^2\alpha\hbar\omega \sum_f |M_{i\to f}|^2 \, \delta(E_f - E_i - \hbar\omega) \qquad (1)$$

where $\hbar\omega$ is the incident photon energy, α is the fine-structure constant, and $M_{i\to f}$ is the transition amplitude between the initial state $|\psi_i\rangle$ of energy E_i and the final state $|\psi_f\rangle$ of energy E_f. In a single particle approach, the many body $|\psi_i\rangle$ and $|\psi_f\rangle$ are replaced by single-particle states. Since we consider K and L_1 edges, $|\psi_i\rangle$ can be either the 1s or the 2s atomic core state in the absence of a core-hole. The final state $|\psi_f\rangle$ in the presence of a core-hole is obtained in an all-electron first-principles calculation.

In a single particle approach and in the electric quadrupole approximation, the transition amplitude is given by the matrix element

$$M_{i\to f} = \langle\psi_f|\mathcal{D}|\psi_i\rangle \qquad (2)$$

with :

$$\mathcal{D} = \hat{\epsilon}\cdot\mathbf{r} + \frac{\mathrm{i}}{2}(\hat{\epsilon}\cdot\mathbf{r})(\mathbf{k}\cdot\mathbf{r}) \qquad (3)$$

where $\hat{\epsilon}$ and $\mathbf{k}$ are the popularization vector and the wave vector of the incident beam and $\mathbf{r}$ is the electron coordinate.

III. X-RAY ABSORPTION CROSS-SECTION IN A PAW FORMALISM

In a first-principles pseudopotential approach, the calculated wavefunction is $|\tilde{\psi}_f\rangle$, namely the pseudowavefunction of the crystal obtained at the end of the self consistent field run. In order to get the all-electron wavefunctions $|\psi_f\rangle$ needed in Eqs. 1, 3, all electron reconstruction needs to be performed. This is achieved in the framework of the PAW method[18]. In this approach the all electron wavefunctions $|\psi\rangle$ are related to the pseudowavefunctions $|\tilde{\psi}\rangle$ though the linear operator $\mathcal{T}$:

$$|\psi\rangle = \mathcal{T}|\tilde{\psi}\rangle \qquad (4)$$

The $\mathcal{T}$ operator is written as a sum of local contributions centered around each atomic site $\mathbf{R}$:

$$\mathcal{T} = 1 + \sum_{\mathbf{R}} \mathcal{T}_{\mathbf{R}} \qquad (5)$$

The local operators $\mathcal{T}_{\mathbf{R}}$ act only within the so-called augmentation regions $\Omega_{\mathbf{R}}$ centered on atomic sites. Following ref.[18], we introduce the all electron (pseudo) partial waves $|\phi_{\mathbf{R},n}\rangle$ ($|\tilde{\phi}_{\mathbf{R},n}\rangle$), and the projector functions $\langle\tilde{p}_{\mathbf{R},n}|$ that satisfy the conditions[25] :

$$\tilde{\phi}_{\mathbf{R},n}(\mathbf{r}) \;=\; \phi_{\mathbf{R},n}(\mathbf{r}) \text{ outside } \Omega_{\mathbf{R}} \qquad (6)$$

$$\left\langle \tilde{p}_{\mathbf{R},n} \middle| \tilde{\phi}_{\mathbf{R}',n'} \right\rangle \;=\; \delta_{\mathbf{R}\mathbf{R}'}\delta_{nn'} \qquad (7)$$

The wavefunctions $|\phi_{\mathbf{R},n}\rangle$ and $|\tilde{\phi}_{\mathbf{R},n}\rangle$ respectively form a basis for valence states, which means that any function $\chi_{\mathbf{R}}$ that vanishes outside Ω_R is expanded as :

$$\sum_n |\tilde{p}_{\mathbf{R},n}\rangle \left\langle \tilde{\phi}_{\mathbf{R},n} \middle| \chi_{\mathbf{R}} \right\rangle = |\chi_{\mathbf{R}}\rangle \qquad (8)$$

Then the operator $\mathcal{T}$ is written as :

$$\mathcal{T} = \mathbf{1} + \sum_{\mathbf{R},n} \left(|\phi_{\mathbf{R},n}\rangle - \left|\tilde{\phi}_{\mathbf{R},n}\right\rangle \right) \langle\tilde{p}_{\mathbf{R},n}| \qquad (9)$$

Substituting eq. 9 in eq. 4 and eq. 4 in eq. 2, leads to :

$$\begin{aligned} M_{i\to f} \;=\; & \left\langle \tilde{\psi}_f \middle| \mathcal{D} \middle| \psi_i \right\rangle + \sum_{\mathbf{R},n} \left\langle \tilde{\psi}_f \middle| \tilde{p}_{\mathbf{R},n} \right\rangle \langle\phi_{\mathbf{R},n}|\mathcal{D}|\psi_i\rangle \\ & - \sum_{\mathbf{R},n} \left\langle \tilde{\psi}_f \middle| \tilde{p}_{\mathbf{R},n} \right\rangle \left\langle \tilde{\phi}_{\mathbf{R},n} \middle| \mathcal{D} \middle| \psi_i \right\rangle \end{aligned} \qquad (10)$$

Since the initial wavefunction ψ_i is localized on the absorbing atom (located at $\mathbf{R}_0$), the terms having $\mathbf{R} \neq \mathbf{R_0}$ can be neglected in eq. 10 to obtain :

$$M_{i\to f} = \left\langle \tilde{\psi}_f \middle| \tilde{\phi}_{\mathbf{R}_0} \right\rangle \qquad (11)$$

with :

$$\left|\tilde{\phi}_{\mathbf{R}_0}\right\rangle = \sum_n |\tilde{p}_{\mathbf{r}_0,n}\rangle \, \langle\phi_{\mathbf{r}_0,n}|\mathcal{D}|\psi_i\rangle \ . \qquad (12)$$

Replacing this matrix element in the XAS cross-section leads to:

$$\sigma(\omega) = 4\pi^2\alpha\hbar\omega \sum_f \left|\left\langle \tilde{\psi}_f \middle| \tilde{\phi}_{\mathbf{R}_0} \right\rangle\right|^2 \delta(E_f - E_i - \hbar\omega) \quad (13)$$

Thus Eq. 13 express the XAS cross-section in terms of single particle states obtained from a pseudopotential calculation. Note that in Eq. 12 there is an infinite number of projectors. Practically only a few projectors are needed to achieve convergence.

IV. XAS IN AN ULTRASOFT PSEUDOPOTENTIAL SCHEME

In an ultrasoft scheme the norm of the pseudo partial waves are different from the norm of the corresponding all-electron partial waves. For this reason it is customary to define[26] the integrated augmentation charges $q_{\mathbf{R},\mathbf{nm}}$ as:

$$q_{\mathbf{R},nm} = \langle \phi_{\mathbf{R},n} | \phi_{\mathbf{R},m} \rangle - \langle \tilde{\phi}_{\mathbf{R},n} | \tilde{\phi}_{\mathbf{R},m} \rangle \quad (14)$$

The the S operator defined in the ultrasoft scheme[24] is then:

$$S = \mathbb{1} + \sum_{\mathbf{R},m,n} |\tilde{p}_{\mathbf{R}n}\rangle q_{\mathbf{R},nm} \langle \tilde{p}_{\mathbf{R}m}| = \mathbb{1} + \sum_{\mathbf{R}} Q_{\mathbf{R}} \quad (15)$$

The pseudo hamiltonian $\tilde{H}$ and the pseudo eigenfunctions $|\psi_f\rangle$ satisfy the following equation[24] :

$$\tilde{H} \left|\tilde{\psi}_f\right\rangle = E_f S \left|\tilde{\psi}_f\right\rangle \quad (16)$$

Multiplication of Eq. 16 by $S^{-1/2}$ leads to :

$$S^{-1/2}\tilde{H}S^{-1/2}S^{1/2} \left|\tilde{\psi}_f\right\rangle = E_f S^{1/2} \left|\tilde{\psi}_f\right\rangle \quad (17)$$

The following identity holds (for a proof see app. A):

$$\pi \sum_f \left|\tilde{\psi}_f\right\rangle \delta(E_f - x) \left\langle \tilde{\psi}_f \right| = \lim_{\gamma\to 0} \Im[\tilde{G}(x)] \quad (18)$$

where x is a real number and

$$\tilde{G}(x) = S^{-1/2} \frac{1}{x - S^{-1/2}\tilde{H}S^{-1/2} - i\gamma} S^{-1/2} \quad (19)$$

Using Eq.13 and 18, the XAS cross section can finally written in a suitable form for a standard Lanczos procedure :

$$\sigma(\omega) = 4\pi\alpha\hbar\omega \lim_{\gamma\to 0} \Im\left[\left\langle \tilde{\phi}_{\mathbf{R}_0} \middle| \tilde{G}(\omega + E_i) \middle| \tilde{\phi}_{\mathbf{R}_0} \right\rangle\right] \quad (20)$$

where E_i is the energy of the initial state that in a pseudopotential scheme is undetermined up to an overall constant. In the case of a unit cell having multiple absorbing sites which are equivalent under the point group symmetry of the crystal, E_i is the same for all the absorbing atoms and the choice of E_i simply corresponds to a rigid shift of the overall spectrum. On the contrary, in the case of nonequivalent absorbing sites in the unit cell, the value of E_i depends on the absorbing site due to the core-level shift. In this case the choice of E_i is not arbitrary and a careful determination of the core-level shift is needed[22]. For simplicity in this work we consider only examples in which there are only equivalent absorbing sites in the unit cell. The determination of the core-level shift in the case of multiple nonequivalent absorbing sites will be given elsewhere. Thus in what follows we choose the energy E_i to be the Fermi level, in the metallic case, the highest occupied state, in the insulating case.

V. LANCZOS PROCEDURE

Eq. 20 can be calculated using the the Lanczos recursion method[27,28,29,30]. The quantity $\langle \tilde{\phi}_{\mathbf{R}_0} | \tilde{G}(E_i + \hbar\omega) | \tilde{\phi}_{\mathbf{R}_0} \rangle$ is evaluated using the continued fraction :

$$\left\langle \tilde{\phi}_{\mathbf{R}_0} \middle| \tilde{G}(E) \middle| \tilde{\phi}_{\mathbf{R}_0} \right\rangle = \cfrac{\left\langle \tilde{\phi}_{\mathbf{R}_0} \middle| \tilde{\phi}_{\mathbf{R}_0} \right\rangle}{a_0 - E - i\gamma - \cfrac{b_1^2}{a_1 - E - i\gamma - \cfrac{b_2^2}{\ddots}}} \quad (21)$$

where the real numbers a_i and b_i are computed recursively by defining the vectors $|u_i\rangle$ such that:

$$|u_0\rangle = \frac{S^{-1/2}\left|\tilde{\phi}_{\mathbf{R}_0}\right\rangle}{\sqrt{\left\langle \tilde{\phi}_{\mathbf{R}_0} \middle| S^{-1} \middle| \tilde{\phi}_{\mathbf{R}_0} \right\rangle}}$$

$$S^{-1/2}\tilde{H}S^{-1/2}|u_i\rangle = a_i|u_i\rangle + b_{i+1}|u_{i+1}\rangle + b_i|u_{i-1}\rangle$$

The a_i and b_i coefficients are defined as:

$$a_i = \left\langle u_i \middle| S^{-1/2}\tilde{H}S^{-1/2} \middle| u_i \right\rangle \quad (22)$$

$$b_i = \left\langle u_i \middle| S^{-1/2}\tilde{H}S^{-1/2} \middle| u_{i-1} \right\rangle \quad (23)$$

This is essentially a standard lanczos process where the initial vector is $|u_0\rangle$ and the Hamiltonian $\tilde{H}$ is replaced by $S^{-1/2}\tilde{H}S^{-1/2}$. However this is not the more efficient way to carry out the lanczos chain since two multiplications by $S^{-1/2}$ are involved and the S matrix is of the same order as the Hamiltonian, namely the dimension is given by the number of plane waves in the calculation (the kinetic energy cutoff). Thus any application of $S^{-1/2}$ costs as much as the application of $\tilde{H}$.

A more efficient way to implement the lanczos process is obtained by defining the auxiliary vectors $|t_i\rangle$, namely:

$$|t_i\rangle = S^{1/2}|u_i\rangle \quad (24)$$

Using this definition, the lanczos process can now directly carried out on the $|t_i\rangle$ vectors as:

$$|t_0\rangle = \frac{\left|\tilde{\phi}_{\mathbf{R}_0}\right\rangle}{\sqrt{\left\langle\tilde{\phi}_{\mathbf{R}_0}\middle|S^{-1}\middle|\tilde{\phi}_{\mathbf{R}_0}\right\rangle}}$$

$$\tilde{H}S^{-1}|t_i\rangle = a_i|t_i\rangle + b_{i+1}|t_{i+1}\rangle + b_i|t_{i-1}\rangle$$

where the new lanczos vectors $|t_i\rangle$ are no longer orthogonal but $\langle t_i|S^{-1}|t_j\rangle = \delta_{i,j}$. If during the lanczos chain the vectors $|\tilde{t}_i\rangle = S^{-1}|t_i\rangle$ are stored then the a_i and b_i coefficients can be defined as:

$$a_i = \left\langle\tilde{t}_i\middle|\tilde{H}\middle|\tilde{t}_i\right\rangle \quad (25)$$

$$b_i = \left\langle\tilde{t}_i\middle|\tilde{H}\middle|\tilde{t}_{i-1}\right\rangle \quad (26)$$

Now, each iteration needs only one multiplication by S^{-1}, one multiplication by $\tilde{H}$, and four lanczos vectors stored in memory, namely $|t_{i-1}\rangle$, $|\tilde{t}_{i-1}\rangle$, $|t_i\rangle$ and $|\tilde{t}_i\rangle$.

To achieve an efficient implementation of the lanczos process, particular care needs to be taken in inverting the S matrix to calculate S^{-1}. Direct inversion of the S matrix is unfeasible being the order of the matrix given by the number of plane waves. Using the definition of S in terms of the N_p ultrasoft projectors, the calculation of S^{-1} can be performed very efficiently by simple products and inversions of matrices of the order of $N_p \times N_P$, as it was demonstrated in refs.[31,32]. In order to have a complete description of the method used we recall the main passages of the demonstration of ref.[31,32] in the appendix B.

VI. APPLICATIONS

The developed method is now applied to silicon and oxygen K-edges in α-quartz, to Cu K-edge in copper and in La_2CuO_4. Density functional theory calculations are performed using the Quantum-Espresso package[33] and the Generalized Gradient Approximation[34]. In the case of La_2CuO_4 we use the Spin Polarized Generalized Gradient Approximation. The developed continued-fraction approach to deal with US pseudopotentials is implemented in the XSpectra package[35] and distributed with the current CVS version of the Quantum-Espresso code. Occupied states are eliminated from the spectrum using the method of ref.[36]. The zero of energy is determined from the self-consistent calculation on a supercell in the presence of a core-hole. In the metallic case we chose the Fermi level while in the insulating case the highest occupied state. It is important to notice that an insulator can become metallic in the supercell calculation due to core-hole attraction. In this case the elimination of the occupied states is somewhat ill defined, as it is in metallic systems. When this occurs, the pre-edge features can be incorrect. This is the case in La_2CuO_4. Further technical details of the calculations are given in each subsection.

A. SiO_2 (α-quartz)

SiO_2 (α-quartz) is a dichroic compound with a hexagonal unit cell and lattice parameters $a = 4.9141\mathring{A}$ and $c = 5.4060\mathring{A}$[37]. The dipolar cross section σ has the following angular dependence[1] :

$$\sigma(\epsilon) = \cos^2(\theta)\sigma_{\parallel} + \sin^2(\theta)\sigma_{\perp} \quad (27)$$

where ϵ is the polarization vector and θ is the angle between the c axis and ϵ.

The charge density calculation was performed with a $2 \times 2 \times 2$ supercell containing 72 atoms. Electronic integration was performed using only the $\mathbf{\Gamma}$ point. We used a 20 Ry kinetic energy cutoff and a 150 Ry cutoff for the charge density, to be compared to the 70 Ry kinetic energy cutoff needed in a standard norm conserving pseudopotentials calculation[17]. The electronic integration in the continued fraction calculation using the lanczos method was performed using a centered $3 \times 3 \times 3$ **k**-points grid of the 72 atoms supercell. Two projectors per channel were used in the PAW reconstruction. The core-hole width was taken constant and set to 0.8 eV for Si K-edge and 1 eV for O K-edge. The continued fraction calculation needed around 400 iterations per **k**-point. We performed a calculation with norm-conserving pseudopotentials in which around 600 iterations were needed for comparable accuracy, like in previous work[1]. Thus the number of iterations needed is smaller, due to the smaller cutoff energy.

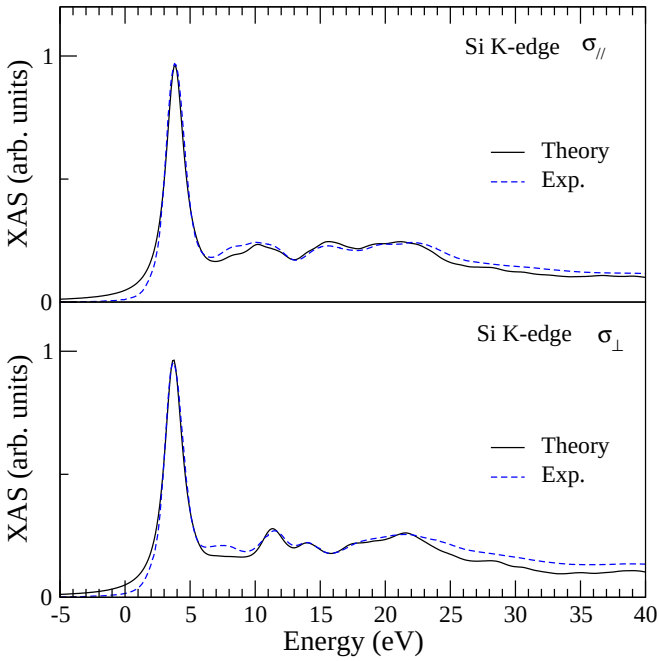

FIG. 1: Experimental[17] and calculated Si K-edge in α-quartz. $\sigma_{\parallel}$ is the polarization along the c axis, while $\sigma_{\perp}$ is the in-plane polarization.

Our results are presented in figures 1 and 2. These results are in perfect agreement with those presented in

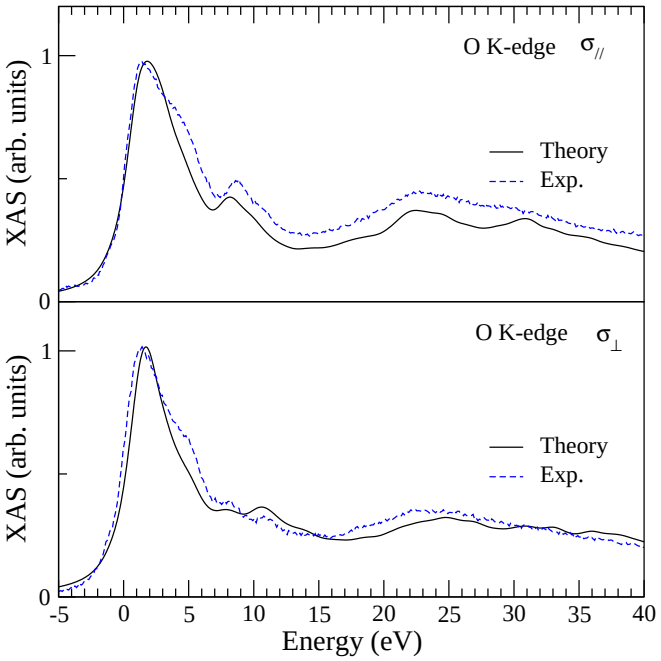

FIG. 2: Experimental[17] and calculated O K-edge in α-quartz. $\sigma_{\parallel}$ is the polarization along the c axis, while $\sigma_{\perp}$ is the in-plane polarization.

ref.[17] and obtained with norm-conserving pseudopotentials. The experimental Si k-edge XAS cross section is very well reproduced for both polarizations despite a too weak peak around 7 eV. A good agreement between theory and experiment for O K-edge is obtained.

The comparison between the ultrasoft pseudopotential and the norm conserving pseudopotential calculations on α-quartz validates our implementation of XAS using ultrasoft pseudopotentials.

B. Copper

Pure copper at room temperature crystallizes in the fcc structure with lattice parameter $3.601\mathring{A}$[38]. The copper K-edge XAS cross section was calculated on a converged $3 \times 3 \times 3$ supercell containing 27 atoms. Electronic integration was performed over a $10 \times 10 \times 10$ uniform k-point grid for both charge density and XAS calculations, with a 30 Ry kinetic energy cutoff and a 500 Ry charge-density cutoff.

The calculated XAS cross section is in good agreement with experimental data (fig. 3). The features A, B, C, D and E are correctly reproduced, however the peak A (shoulder) is shifted of about 1 eV to higher energies. This shift is also present in finite difference method calculations[40]. Since copper is metallic, the description of the A peak is difficult, because the core-hole attraction can drag some states below the Fermi energy.

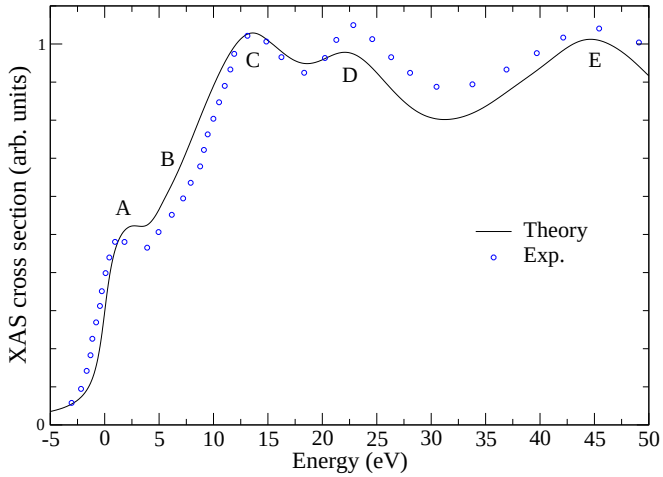

FIG. 3: Calculated Cu K-edge in copper compared to experimental data from ref.[39]. The Lorentzian γ broadening parameters is variable and runs from 1 to 4 eV.

C. La_2CuO_4

La_2CuO_4 is the parent compound of high Tc superconductors. It is an antiferromagnetic correlated insulator considered a challenge for density functional theory. Furthermore it requires large cutoff energies to be simulated with norm-conserving pseudopotentials. Thus it is an ideal test for our approach.

At low temperatures La_2CuO_4 present an weak orthorhombic distortion of the tetragonal structure. In our calculation we neglect the orthorhombic distortion and consider the tetragonal structure having $a = 5.357$ Åand $c = 13.143$ Å[41]. Under this assumption, the Cu K-edge XAS dipolar cross section can be described as a linear combination of the cross-section having in-plane polarization ($\sigma_{\perp}$) and of that having polarization along the c-axis ($\sigma_{\parallel}$),as expressed in eq. 27.

We treat correlation effects the framework of the the spin polarized GGA+U[34,42] approximation, where U is the Hubbard parameter on Cu 3d states. The U parameter is 9.6 eV, as calculated from first principles using a linear response scheme[42,43]. We use ultrasoft pseudopotentials for all atomic species leading to a 30 Ry kinetic energy cutoff and a 200 Ry charge density cutoff. The kinetic energy cutoff used with ultrasoft pseudopotentials has to be compared with the more than 150 Ry kinetic energy cutoff needed in the case of norm conserving pseudopotentials. We use two PAW projectors per channel and non-linear core correction in the Cu pseudopotential. By calculating XAS on the antiferromagnetic unit cell we have checked that the inclusion of semicore states does not affect the result. We used a $1 \times 1 \times 1$ supercell of the antiferromagnetic crystal cell containing 14 atoms. For the electronic integration we use a uniform $6 \times 6 \times 6$ k-point mesh both for the charge density and for the continued fraction calculation. We have verified that the result is unaffected by the use of larger supercells.

Experimentally, La_2CuO_4 is an insulator with a gap around 2 eV[44], and exhibits an antiferromagnetic order[45] with a magnetic momentum on copper atoms around $0.5\mu_B$. Our CGA+U electronic structure calculation gives a 0.5 eV charge-transfer gap and a magnetization of $0.58\mu_B$.

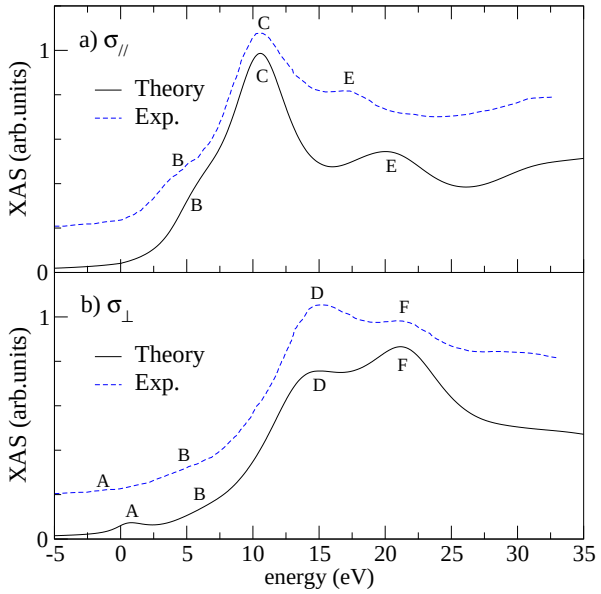

FIG. 4: Experimental[46] and calculated Cu K-edge in La_2CuO_4. The calculated cross section was obtained with a U=9.6 eV parameter on Cu 3d states. The Lorentzian γ broadening parameters varies linearly between 1 eV in the pre-edge region and 4 eV in the far-edge region. $\sigma_\parallel$ indicates the polarization along the c axis while $\sigma_\perp$ the in-plane one.

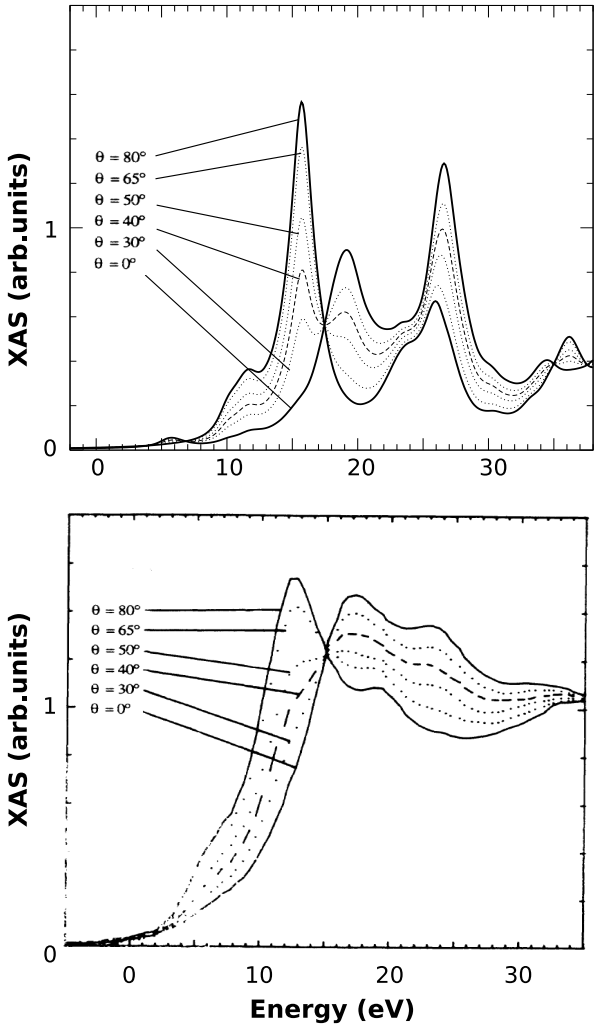

FIG. 5: Angular dependence of La_2CuO_4 Cu K-edge XAS dipolar cross section compared with experimental data[46]. The angle between the CuO_2 layer and the c-axis is labeled θ, so that $\theta = 90^o$ corresponds to ϵ along the c-axis. The Lorentzian γ broadening parameters is 0.8 eV. The core-hole width has been artificially reduced in the calculation to show the presence of different peaks.

The results of the CGA+U Cu K-edge XAS calculations are presented in fig. 4. When the polarization is parallel to the CuO_2 planes the energy position of the different peaks is well reproduced by our calculation. In particular B, D,and F are at the correct energy position, however the intensity of peak D is underestimated. In the pre-edge region the peak A is shifted to higher energy. The A peak is not well described in our calculation since, due to the underestimation of the electronic gap and overestimation of core-hole attraction, the system becomes metallic when a core-hole is included in the calculation. In particular, while the system in the absence of a core-hole is insulating, when we add the core-hole in the supercell calculation, we obtain a metallic system. As a consequence it becomes impossible to distinguish between occupied and empty states. The intensity of peak A is crucially affected. The system is formally in a $|3d^{10}\underline{L}\rangle$ state with no empty d-states and consequently no quadrupolar pre-edge. On the contrary it is known that a weak quadrupolar pre-edge is present in experiments[3].

The nature of peak B has been widely discussed. It has been alternatively assigned to shakedown $1s^2 3d^9 L \longrightarrow 1s^1 3d^{10}\underline{L}$ processes[47], and to empty p states of the absorbing atom[46,48]. Here we unambiguously attribute the peak B to empty p states and thus this excitation is single particle in nature.

In the spectra having polarization along the c-axis the intensities are in better agreement with experimental data. However the peak E is substantially shifted to higher energies (3 eV). More insight on this issue can be obtained by considering the angular dependence of the spectra and by comparing it to available experimental data[46], as shown in Fig.5.

In the theoretical calculation of Fig. 5 we have substantially reduced the peak linewidth to 0.8 eV to emphasize the multi structured form of the different peaks. In particular it is seen that the peak at 20 eV (labeled peak E in Fig. 4) is actually composed of two different peaks. The high energy one is at the correct energy posi-

tion while the low energy one is shifted to higher energy with respect to the experiment. The incorrect position of the lowest energy peak substantially affects the intensity in the 10-20 eV region for both polarizations and is responsible for the disagreement with the experimental data. Indeed if this peak was at low energy the intensity of peak D in Fig. 4) would also increase and a better agreement with experiment would be obtained for both polarizations.

Kosugi et al.[48] attributed the decoupling of pre-edge and near-edge features present in K-edge XAS on powder samples to charge-transfer multi-determinant effects. In particular it was shown that the main edge and the B peak are decoupled in the isotropic spectra. However the pre-edge and edge structures occur at different energies when the polarization is in the plane or out of plane. We find that the decoupling indeed originates from the average over different polarization of the single-particle spectra. Thus the doubling of edge and pre-edge peaks are not due to multi-determinant charge transfer effects.

Tolentino et al.[46] assigned peaks C and E to $3d^{10}\underline{L}$ transitions, and peaks D and F to $3d^9L$ transitions, implying that the XAS spectrum includes multi-determinant effects. If this would be the case, being our calculation single determinant in nature, a single peak should be seen in both directions. This is however not the case and our calculation correctly reproduces the main experimental features except for an energy shift for the peak E. Consequently the near-edge and far-edge structures detected in K-edge XAS of La_2CuO_4 are all single particle in origin. Concerning the E peak, it corresponds to a single particle excitation that is 3 eV shifted with respect to experiments. This shift can be due to an incorrect description of the hybridization between Cu 4p states of the absorbing atom and La states. La states are indeed hard to describe in a single particle approach for their intrinsic correlated nature. We believe that, despite the 3 eV shift of the E-peak, the single particle origin of the C,D,E,F peaks is definitely clarified. To have better insight on the subject it would be interesting to study the case of $Ca_{2-x}CuO_2Cl_2$[49] since no rare-earths are present in the system and consequently the E peak should be at the right position.

VII. CONCLUSION

A DFT-based continued fraction method using ultrasoft pseudopotentials to calculate the X-ray absorption spectra is presented. Our implementation, relying on ultrasoft pseudopotentials, is an order of magnitude faster than preceding implementations based on norm-conserving one[4,17]. Indeed the bulk of the calculation is the determination of the self-consistent charge density for a supercell in the presence of a core-hole. Since Ultrasoft pseudopotentials allow for substantially smaller cutoffs, the computation cost is strongly reduced. Furthermore the number of iteration in the continued fraction is reduced and convergence is then faster than the norm-conserving case.

We validate the method by calculating silicon and oxygen K-edges of alpha-quartz, Cu k-edge in bulk metallic copper and Cu K-edge in La_2CuO_4. In the case of weak to intermediate correlation (silicon and oxygen K-edges of alpha-quartz and Cu K-edge in metallic copper) we obtain a good agreement with experimental data. The description of XAS spectra of strongly correlated compounds as La_2CuO_4 is typically considered a challenge for DFT-based method. Nevertheless we were able to attribute all the single particle peaks (B, C, D, F in Fig. 4). We then solve the long-standing[46,47,48] discussion on the attribution of the near-edge and far-edge features in La_2CuO_4.

VIII. ACKNOWLEDGEMENTS

We acknowledge fruitful discussion with A. M. Saitta, R. Gebauer, D. Cabaret, Ch. Brouder, Ph. Sainctavit, N. Marzari and D. Ceresoli. Calculations were performed at the IDRIS supercomputing center (project 081202).

APPENDIX A: PROOF OF EQ. 18

We proof that for x real number the following holds:

$$\begin{aligned}&\pi\sum_f \left|\tilde{\psi}_f\right\rangle \delta(E_f-x)\left\langle\tilde{\psi}_f\right| = \\ &= \lim_{\gamma\to 0}\Im\left[S^{-1/2}\frac{1}{x-S^{-1/2}\tilde{H}S^{-1/2}-i\gamma}S^{-1/2}\right].\end{aligned} \tag{A1}$$

Since

$$\begin{aligned}&\pi\sum_f \left|\tilde{\psi}_f\right\rangle \delta(E_f-x)\left\langle\tilde{\psi}_f\right| = \\ &= \lim_{\gamma\to 0}\Im\left[\sum_f \left|\tilde{\psi}_f\right\rangle \frac{1}{x-E_f-i\gamma}\left\langle\tilde{\psi}_f\right|\right]\end{aligned} \tag{A2}$$

we have

$$\begin{aligned}&\sum_f \left|\tilde{\psi}_f\right\rangle \frac{1}{x-E_f-i\gamma}\left\langle\tilde{\psi}_f\right| = \\ &= \sum_f S^{-1/2}\frac{1}{x-E_f-i\gamma}S^{1/2}\left|\tilde{\psi}_f\right\rangle\left\langle\tilde{\psi}_f\right| \\ &= \sum_f S^{-1/2}\frac{1}{x-S^{-1/2}\tilde{H}S^{-1/2}-i\gamma}S^{1/2}\left|\tilde{\psi}_f\right\rangle\left\langle\tilde{\psi}_f\right| \\ &= S^{-\frac{1}{2}}\frac{1}{x-S^{-\frac{1}{2}}\tilde{H}S^{-\frac{1}{2}}-i\gamma}S^{-\frac{1}{2}}\sum_f S\left|\tilde{\psi}_f\right\rangle\left\langle\tilde{\psi}_f\right| \\ &= S^{-1/2}\frac{1}{x-S^{-1/2}\tilde{H}S^{-1/2}-i\gamma}S^{-1/2}\end{aligned}$$

where in the last equality we used the following property[24]:

$$\mathbb{1} = \sum_f \left|\tilde{\psi}_f\right\rangle \left\langle\tilde{\psi}_f\right| S = \sum_f S \left|\tilde{\psi}_f\right\rangle \left\langle\tilde{\psi}_f\right|. \quad \text{(A3)}$$

Eq. A1 follows from eq. A3.

APPENDIX B: CALCULATING THE S^{-1} MATRIX

Following ref.[24], the S matrix can be written as :

$$S = \mathbb{1} + \sum_{i,j} q_{ij} \left|\tilde{p}_i\right\rangle \left\langle\tilde{p}_j\right| \quad \text{(B1)}$$

where i and j are cumulative indexes for $\mathbf{R}m$ and $\mathbf{R}n$, respectively. We assume that S^{-1} can be written as:

$$S^{-1} = \mathbb{1} + \sum_{i,j} a_{ij} \left|\tilde{p}_i\right\rangle \left\langle\tilde{p}_j\right| \quad \text{(B2)}$$

The S^{-1} matrix satisfies the equation $SS^{-1} = \mathbb{1}$:

$$\begin{aligned} SS^{-1} &= (\mathbb{1} + \sum_{i,j} q_{ij} \left|\tilde{p}_i\right\rangle \left\langle\tilde{p}_j\right|)(\mathbb{1} + \sum_{l,m} a_{lm} \left|\tilde{p}_l\right\rangle \left\langle\tilde{p}_m\right|) \\ &= \mathbb{1} + \sum_{i,j} \left|\tilde{p}_i\right\rangle \left\langle\tilde{p}_j\right| (q_{ij} + a_{ij} + \sum_{lm} q_{ij} P_{jl} a_{lm}) \end{aligned} \quad \text{(B3)}$$

where $P_{jl} = \langle\tilde{p}_j|\tilde{p}_l\rangle$. In matrix form the equation is:

$$q + a + qPa = 0 \quad \text{(B4)}$$

whose solution is $a = -(1 + qP)^{-1}Q$. Thus S^{-1} can be calculated by inverting matrices of the size of $N_P \times N_P$, where N_P is the number of ultrasoft projectors. A similar procedure was used in ref.[31,32].

[1] C. Brouder, J. Phys. Cond. Mat. **2**, 701-738 (1990)
[2] F. de Groot and A. Kotani, *Core Level Spectroscopy of Solids*, Taylor and Francis, 2008
[3] A. Shukla, M. Calandra, M. Taguchi, A. Kotani, G. Vanko and S.-W. Cheong, Phys. Rev. Lett. **96**, 077006 (2006)
[4] C. Gougoussis, M. Calandra, A. Seitsonen, Ch. Brouder, A. Shukla, and F. Mauri, Phys. Rev. B **79**, 045118 (2009)
[5] A. Juhin, G. Calas, D. Cabaret, L. Galoisy and J.-L. Hazemann, Phys. Rev. B **76**, 054105 (2007)
[6] P. Wernet, D. Nordlund, U. Bergmann, M. Cavalleri, M. Odelius, H. Ogasawara, L. A. Naslund, T. K. Hirsch, L. Ojamae, P. Glatzel, L. G. M. Pettersson, A. Nilsson, Science **304**, 995-999 (2004)
[7] R. L. C. Wang, H. J. Kreuzer and M. Grunze, Phys. Chem. Chem. Phys. **8**, 4744 - 4751 (2006)
[8] J. D. Smith, C. D. Cappa, B. M. Messer, W. S. Drisdell, R. C. Cohen and R. J. Saykall, J. Phys. Chem. B **110**, 2003820045 (2006)
[9] D. Prendergast and G. Galli, Phys. Rev. Lett. **96**, 215502 (2006)
[10] T. Head-Gordon and M. E. Johnson, PNAS **103**, 7973-7977 (2006)
[11] G. Brancato, N. Rega and V. Barone, Phys. Rev. Lett. **100**, 107401 (2008)
[12] R.D. Cowan, The theory of atomic structure and spectra, University of California Press (1981)
[13] C. R. Natoli,D. K. Misemer, S. Doniach and F. W. Kutzler, Phys. Rev. A **22**, 1104–1108 (1980)
[14] L. Fonda, J. Phys. Cond. Mat. **4**, 8269-8302 (1992)
[15] L. A. Ankudinov, B. Ravel, J. J. Rehr and S. D. Conradson, Phys. Rev. B **58**, 7565–7576 (1998)
[16] E. L. Shirley, Phys. Rev. Lett. **80**, 794 (1998)
[17] M. Taillefumier, D. Cabaret, A.-M. Flank and F. Mauri, Phys. Rev. B **66**, 195107 (2002)
[18] P. E. Blöchl, Phys. Rev. B **50**, 17 953 (1994)
[19] Hetényi B., De Angelis F., Giannozzi P., and Car R., J. Chem. Phys. **120**, 8632 (2004)
[20] C. J. Pickard and M. C. Payne, Electron Microscopy and Analysis **153**, 179 (1997)
[21] P. Rez, J. R. Alvarez, and C. J. Pickard, Ultramicroscopy, bf 78 175 (1999)
[22] Gao S. P., Pickard C. J., Payne M. C., Zhu J., Yuan J., Phys. Rev. B **77**, 115122 (2008)
[23] V. I. Anisimov, J. Zaanen and O. Andersen, Phys. Rev. B **44**, 943–954 (1991)
[24] D. Vanderbilt, Phys. Rev. B **41**, 7892–7895 (1990)
[25] The solutions of the radial Schrödinger equations for the isolated atom are a natural choice for the all electron partial waves.
[26] J. R. Yates, C. J. Pickard, F. Mauri, Phys. Rev. B **76**, 024401 (2007)
[27] C. Lanczos, J. Res. Natl. Bur. Stand. **49**, 33 (1952)
[28] C. Lanczos, J. Res. Natl. Bur. Stand. **45**, 255 (1950)
[29] R. Haydock, V. Heine and M. J. Kelly, J. Phys. C: Solid State Physics **5**, 2845-2858 (1972)
[30] R. Haydock, V. Heine and M. J. Kelly, J. Phys. C: Solid State Physics **8**, 2591-2605 (1975)
[31] P. J. Hasnip and C. J. Pickard, Computer Physics Communications, **174**, 24 (2006)
[32] B. Walker and R. Gebauer, J. Chem. Phys. **127**, 164106 (2007)
[33] P. Giannozzi et al., http://www.quantum-espresso.org
[34] J.P.Perdew, K.Burke, M.Ernzerhof, Phys. Rev. Lett. **77**, 3865 (1996)
[35] The XSpectra package by C. Gougoussis, M. Calandra, A. Seitsonen and F. Mauri is available under the gnu license in the current CVS version of the Quantum Espresso code.
[36] Ch. Brouder, M. Alouani and K. H. Bennemann, Phys. Rev. B **54**, 7334–7349 (1996)
[37] G. A. Lager, J. D. Jorgensen and F. J. Rotella, Journal of Applied Physics **53**, 6751-6756 (1982)
[38] H.M. Otte, Journal of Applied Physics **32**, 1536-1546 (1961)
[39] C. T. Chantler, C. Q. Tran, Z. Barnea, D. Paterson, D. J.

Cookson and D. X. Balaic, Phys. Rev. A **64**, 062506 (2001)
[40] Y. Joly, Phys. Rev. B **63**, 125120 (2001)
[41] M. Reehuis, C. Ulrich, K. Prokes, A. Gozar, G. Blumberg, Seiki Komiya, Yoichi Ando, P. Pattison and B. Keimer, Phys. Rev. B **73**, 144513 (2006)
[42] M. Cococcioni and S. de Gironcoli, Phys. Rev. B **71**, 035105 (2005)
[43] H.J. Kulik, M. Cococcioni, D. A. Scherlis and N. Marzari, Phys. Rev. Lett. **97**, 103001 (2006)
[44] J. M. Ginder, M. G. Roe, Y. Song, R. P. McCall, J. R. Gaines, E. Ehrenfreund, and A. J. Epstein, Phys. Rev. B **37**, 7506–7509 (1988)
[45] D. Vaknin, S. K. Sinha, D. E. Moncton, D. C. Johnston, J. M. Newsam, C. R. Safinya and H. E. King, Phys. Rev. Lett.**58**, 2802–2805 (1987)
[46] H. Tolentino, M. Medarde, A. Fontaine, F. Baudelet, E. Dartyge, D. Guay and G. Tourillon, Phys. Rev. B **45**, 8091 (1992)
[47] R. Bair and W. Goddard, Phys. Rev. B **22** 2767–2767 (1980)
[48] N. Kosugi, Y. Tokura, H. Takagi and S. Uchida, Phys. Rev. B **41**, 131–137 (1990)
[49] I. Yamada, A. A. Belik, M. Azuma, S. Harjo, T. Kamiyama, Y. Shimakawa, and M. Takano, Phys. Rev. B **72**, 224503 (2005)
[50] The presence of a core-hole in the pseudopotential of the absorbing atom reduce the symmetry of the crystal.